Advances in Understanding of Bluff Body Wakes and Vortex-Induced Vibration, Washington DC, June 1998.

LDV-measurements in the near wake of a circular cylinder

C. Norberg

Division of Heat Transfer, Lund Institute of Technology, P.O. Box 118, S-221 00, LUND, Sweden (chris@ms.vok.lth.se)

Abstract

Results from LDV-measurements in the near wake of a high-aspect-ratio circular cylinder in low-blockage cross flow are presented (aspect ratio 65, blockage 1.5%). Reynolds numbers from $Re = 1.5 \times 10^3$ to $Re = 10 \times 10^3$ are covered. Statistical moments (mean, RMS and skewness) are presented for the streamwise and spanwise velocity components, respectively. Length scales are identified from positions of extreme values for these quantities. For $Re < 8 \times 10^3$ the RMS-distribution of streamwise velocity along the wake centerline has two local maxima, as opposed to higher Re where only one maximum is identified. With an increase in Re over the range covered there is a significant upstream movement of critical points. For instance, the upstream movement of the mean wake closure point is about 0.8 diameters (from about 2.3 diameters behind the cylinder axis at $Re = 1.5 \times 10^3$ to about 1.5 diameters at $Re = 10 \times 10^3$). Traverses across the wake at 0.6, 1 and 2 diameters downstream of the cylinder axis are also carried out. Within this short distance the distribution of streamwise velocity defect changes from a near top-hat to a Gaussian type of profile. Reasons for the occurrence of a fundamental transition in the near wake in between $Re = 5 \times 10^3$ and $Re = 8 \times 10^3$ are discussed.

1 Introduction

In Linke (1931) [21] an extensive near wake study within the Re-range from about 1.5×10^3 to 15×10^3 is presented. His careful Pitot-tube measurements reveal that there is, in between $Re = 1.5 \times 10^3$ and $Re = 10 \times 10^3$, a considerable shrinking of the recirculating region behind the cylinder (by about one diameter which corresponds to an approximate 50% decrease when measured from the axis of the cylinder). Associated with this shrinking process, Linke also observes a significant upstream movement of the transitional point in the separated shear layers, a feature which later (1964) was investigated thorough by Bloor [7].

From previous measurements [43, 31] it is indicated that the shedding process is extremely weak at around $Re = 1.5 \times 10^3$, coinciding with local extreme values for the Strouhal number [32], the base suction coefficient [32] and the RMS lift coefficient [31], respectively. In between $Re = 1.5 \times 10^3$ and $Re = 15 \times 10^3$ there is an approximate tenfold increase in the RMS lift coefficient [31] whereas the Strouhal number drops by only about 7% [32]. Further, at around $Re = 1.5 \times 10^3$, as discovered by Bloor [7] in 1964, shear-layer vortices [50] show up as important ingredients in the near wake, see Prasad & Williamson (1997a) [35]. These structures develops in the separating shear layers by the action of a Kelvin-Helmholtz instability mechanism [35].

As shown in Norberg (1987) [28] there is an abrubt change in the appearance of the vortex shedding frequency occurring at around $Re = 5 \times 10^3$; below this critical value (down to about $Re = 260$) the shedding peak is of extremely high quality whereas at higher values (up to about $Re = 2 \times 10^5$) the shedding peak is significantly broader indicating that the shedding frequency varies with time (as shown e.g. in [6]). Later flow visualizations, e.g. [30, 31], show that this transitional behaviour is related to a fundamental change in the three-dimensional evolution of Kármán vortices. At Reynolds numbers below this critical value (probably all the way down to $Re \simeq 260$), the Kármán vortices are surprisingly straight and aligned with the cylinder axis whereas for higher Re the vortices exhibit much more undulation with occasional ingredients of vortex dislocation, e.g. see [30, 31]. Confirmation of this behaviour including further evidence of large-scale phase dislocations along the span occurring above some critical Re close to $Re = 5 \times 10^3$ can be found in Prasad & Williamson (1997b) [36]. In [36] the transition is observed only under conditions where parallel shedding is attempted (both end plates tilted and pointing upstream). At this point, it needs to be reiterated that the transition has been shown to occur also under conditions using ordinary non-tilted end plates [31]. For sufficiently large aspect ratios (greater than about $L = 50$) the transitional process appears to be independent of this parameter, see [31].

The sudden increase in the relative bandwidth occurs at $Re \simeq 5.1 \times 10^3$ for $Tu = 0.06\%$ and at $Re \simeq 4 \times 10^3$ for $Tu = 1.4\%$ (grid-generated), respectively, see [28, 29]. The relative bandwidth then increases up to local maximum at a second critical Re, which for $Tu = 0.06\%$ occurs at $Re \simeq 7.5 \times 10^3$

[31]. At around this second critical Re there is a plateau in the variation of the base suction coefficient *vs.* Re, see [32]. These measurements were not carried out in the same wind tunnel as in the present study. However, from the author's preliminary studies on aspect-ratio effects using the present wind tunnel, the same transitional behaviour as described above was noted. The only difference was that the inception of increasing shedding bandwidth then occurred at a somewhat lower Reynolds number ($Re \simeq 4.6 \times 10^3$). In addition, for sufficiently large aspect ratios ($L \geq 50$) using non-tilted end plates, the above-mentioned plateau for ($-C_{pb}$) was noted also in these preliminary tests.

Obviously, within the considered range of Re, i.e. from $Re = 1.5 \times 10^3$ to 10×10^3, there are mechanisms which have a significant influence on the strength and subsequent roll-up of the Kármán vortices as well as on intrinsic three-dimensional large-scale flow features. Probably, these mechanisms are related to interactions between the primary Kármán vortices, the shear layer vortices and the essentially streamwise (longitudinal) mode B type of secondary vortices, which occur along the span roughly with a spanwise wavelength of about one cylinder diameter [49, 20].

The present paper presents experimental data on the streamwise and spanwise velocity components in the near wake, using the technique of Laser Doppler Velocimetry, LDV. When used correctly, this technique can provide accurate and reliable data within this highly turbulent and recirculating region, see McKillop & Durst (1984) [24]. The main purpose was to gather and analyse such data with a high spatial resolution. The prospective was that the results then could provide some relevant information regarding transitional flow features in the near wake. Hopefully, the results can be used as comparison data within the rapidly increasing field of Computational Fluid Dynamics (CFD), see e.g. Beaudan & Moin (1994) [4].

2 Experimental Details

All measurements were carried out in the closed-circuit low-speed wind tunnel L1 at the Department of Fluid and Thermo Dynamics (Chalmers University of Technology, Gothenburg). The working section is 2.9 m long and has a rectangular cross-section of height 0.5 m and width 0.4 m. For the flow speeds considered in this study the free stream turbulence intensity is less than 0.1% (2 Hz to 5000 Hz). The acoustic noise level is less than 1% of the dynamic pressure [27], a level completely dominated by fluctuations at frequencies less than 85 Hz. The lowest shedding frequency in the present tests was about 135 Hz. As shown in Peterka & Richardson (1969) [34], high sound levels at around the natural shear layer frequency, which is always greater than the shedding frequency [7], can cause interactions with the developing flow field but when disturbances are well below the shedding frequency no effects can be noted. The lowest shear layer frequency in the present tests was about 450 Hz. The cylinder had a diameter of $d = 6.0$ mm and was made of solid stainless steel of high quality and surface finish. It was oriented vertically and was mounted rigidly at a symmetric position with respect to the side walls. The cylinder was equipped with thin circular end plates having a diameter of ten times the cylinder diameter. The distance between the end plates was 390 mm thus providing an aspect ratio of 65. The clearance distance between the walls and the end plates was about 50 mm. From previous investigations by the author using hot wires it is known that the thickness of the boundary layers on the tunnel walls at the cylinder position is about $20 - 30$ mm. Outside these layers the velocity is constant within $\pm 0.3\%$. All measurements were carried out at the midspan position. The blockage ratio was 1.5%.

A commercial (Dantec) fibre-optic LDV-system arranged in a backscatter mode was employed (focal length, 310 mm). For measurements of the streamwise ($\tilde{U}$) and spanwise ($\tilde{W}$) velocity components, respectively, the green (wavelength 514.5 nm) and the blue (488 nm) coherent lights of an argon-ion laser (Coherent Innova model 90-4) was used. The probe with a beam expander of factor 1.94 contained both transmitting and receiving optics, and the signals from the photomultipliers were analyzed using two burst spectrum analyzers (Dantec 57N10). That the four light beams crossed each other in the same point was checked separately with a tiny aperture mounted on an optical bench. From measurements of the beam angles the sensitivity factors for the velocity components $\tilde{U}$ and $\tilde{W}$ were 4.12 $(m/s)/MHz$ and 3.85 $(m/s)/MHz$, respectively (beam half-angles approx. 3.6°). The free stream velocity (U_∞) was determined from repeated measurements at a position 160 mm (27 diameters) upstream of the cylinder. When scaled with U_∞ the spanwise velocity at this position was within ± 0.003. The ellipsoidal measurement volumes were each approx. 0.05 mm in width and 0.5 mm in length. The seeding droplets (Invent Safex-Inside-Nebelfluide SUPER) were generated using a 6-jet atomizer (TSI model 8306-6), which was located downstream of the cylinder. Validated burst rates of typically (1.0/0.5) kHz (green/blue) were obtained. The number of samples collected at each position was typically 10,000 ($\tilde{U}$) and 5,000 ($\tilde{W}$), respectively. Transit time weighting for bias correction was applied to the data. The respective noise

levels for $\tilde{U}$ and $\tilde{W}$ were approx. 1.6% and 1.0% of the free stream velocity. The computer-controlled 3D-traverse system had a positional accuracy of about 35 μm with a resolution of about 2 μm.

Except otherwise stated, all positions and length scales are scaled with the cylinder diameter d, velocities with the free stream velocity U_∞, and frequencies with U_∞/d. The origin of the coordinate system was placed at the cylinder axis (midspan position). The streamwise and cross-stream directions are denoted x and y, respectively. The wake centerline ($y = 0$) was found from symmetry of measured streamwise velocity variations across the wake. The traverse system then was aligned with this line, with an alignment error which was estimated to be less than 1.5°. After this procedure, the streamwise center of the cylinder ($x = 0$) was found from the two positions ($x = \pm 1/2$) where the laser beams touched the cylinder surface. The uncertainty in U was estimated to be ± 0.006. Corresponding uncertainties for RMS-velocities u_{RMS} and w_{RMS} were ± 0.02 and ± 0.03, respectively.

3 Results and Discussion

3.1 Wake centerline

A summary of critical values from measurements along the wake centerline ($y = 0$, $x > 0.5$) is compiled in Table 1. The underlying data is depicted in Fig. 1. With an increase in Re from 1.5×10^3 to 10^4 there was a decrease of about 34% in the wake closure length ℓ_c. All other length scales in Table 1 followed the same pattern of decrease. The variation of mean streamwise velocity $U(x, 0)$ showed a consistent decrease towards zero velocity when approaching the base of the cylinder (at $x = 0.5$). However, the absolute value for the wall gradient was about 5 times higher at $Re = 10 \times 10^3$ as compared to $Re = 1.5 \times 10^3$, the gradient being approximately equal to -1.2 at $Re = 10 \times 10^3$. Also the variation of u_{RMS} when approaching the base showed a consistent decrease towards zero. However, at around $x = 0.6$ for the spanwise RMS velocity there was a departure from a steady decrease towards $w_{RMS} = 0$ at the base, see Fig. 1(d). This was believed to be an effect caused by the finite measurement volume.

$Re/10^3$	ℓ_U	U_{min}	ℓ_c	$\ell_u^{(1)}$	$\hat{u}_{RMS}^{(1)}$	$\ell_u^{(2)}$	$\hat{u}_{RMS}^{(2)}$	ℓ_S	ℓ_w	$\hat{w}_{RMS}$
1.5	1.75	−0.40	2.29	1.51	0.30	2.23	0.32	1.86	2.08	0.36
3.0	1.65	−0.44	2.16	1.45	0.33	2.09	0.34	1.72	1.86	0.39
5.0	1.42	−0.45	1.90	1.23	0.35	1.83	0.36	1.50	1.61	0.39
8.0	1.17	−0.35	1.67	(1.02)	(0.37)	1.62	0.45	1.32	1.41	0.39
10.	1.04	−0.38	1.52	(0.96)	(0.37)	1.50	0.43	1.18	1.26	0.39

Table 1: Summary of critical values along the wake centerline, $y = 0$.

Interestingly, for $Re < 8 \times 10^3$ the distributions of RMS streamwise velocity exhibited two distinct peaks whereas only one such peak was present for higher Re, see Fig. 1(b). For $Re \geq 8 \times 10^3$ there was instead an inflexional appearance at $x \simeq 1$ (associated values are within parentheses in Table 1). Although being within the experimental accuracy, the second maximum, $\hat{u}_{RMS}^{(2)}$, appeared to be the highest one ($Re < 8 \times 10^3$). The highest RMS streamwise velocity always occurred slightly upstream of the mean wake closure point. For w_{RMS} only one local maximum along $y = 0$ could be detected (at $x = \ell_w$).

The secondary peak for u_{RMS} along $y = 0$ is believed to be caused by the cross-over of mode B type of secondary structures. As shown in Wu *et al.* (1993) [48] the velocity perturbations induced by the passage of these longitudinal vortices are of the order 0.3 times the free stream velocity. The extreme constancy of the shedding frequency and the very small undulations of Kármán vortices in the spanwise direction in between $Re \simeq 260$ and $Re \simeq 5 \times 10^3$ [31] implies an extreme regularity within the near-cylinder wake region, a region where these structures are generated [10, 16]. Above the transition at $Re \simeq 5 \times 10^3$ there is significant spanwise undulation of the Kármán vortices with occasional dislocations and a much less regular shedding frequency [31]. Under these non-regular conditions in the base region the secondary peak is expected to be smeared out.

It is important to point out that also results from measurements using standard hot wire anemometry along $y = 0$ indicate a change of appearance within this range of Reynolds number, see Norberg (1987) [28] and Prasad & Williamson (1997a) [36]. From these studies the mean *cooling* velocity at Reynolds numbers below the indicated inception of vortex dislocations can be seen to exhibit a distinct plateau slightly upstream of the position for maximum RMS *cooling* velocity, whereas not so at higher Re. For the RMS *cooling* velocity only one maximum is noted, see [28, 36].

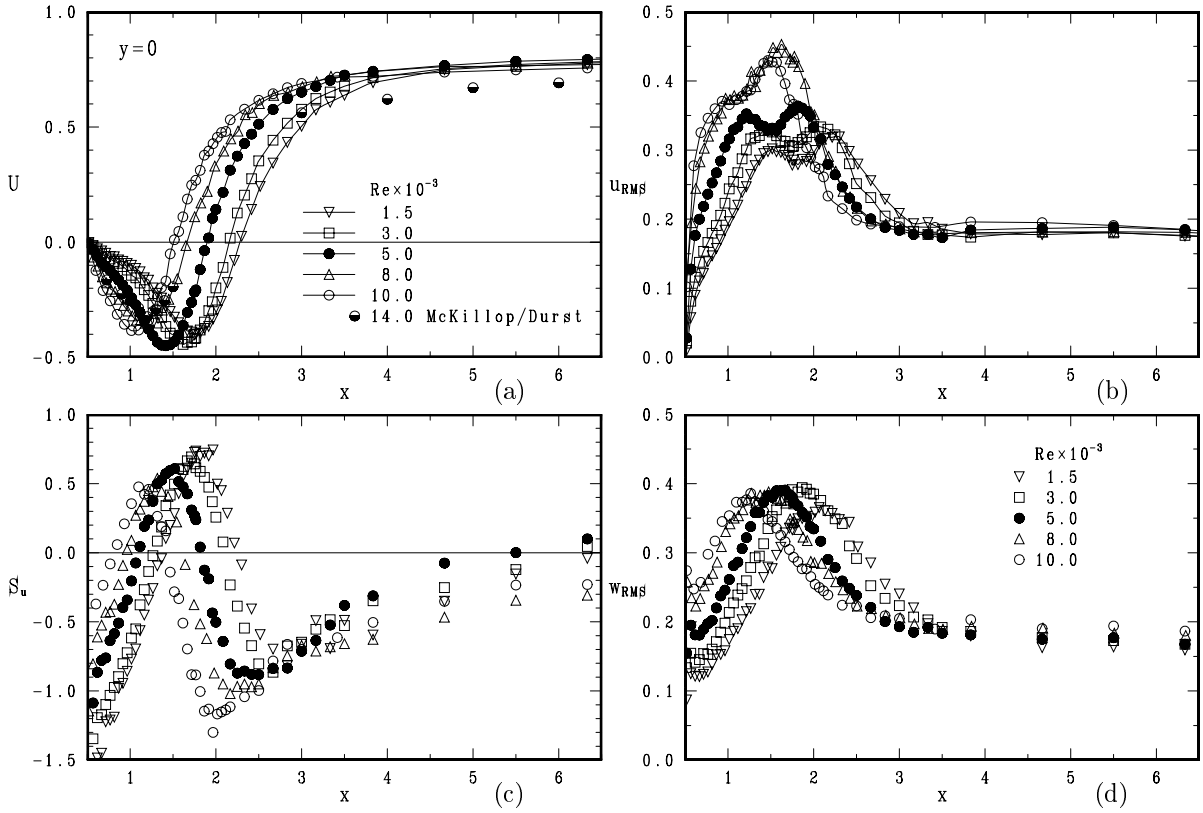

Figure 1: Results from measurements along the wake centerline. (a) mean streamwise velocity, (b) RMS streamwise velocity, (c) skewness factor of streamwise velocity fluctuations, (d) RMS spanwise velocity.

In the present study, both ℓ_c and $\ell_u^{(2)}$ were used as a measure for the vortex formation length ℓ_f, see Fig. 2(a). For clarifications of past definitions of the formation length the reader is referred to e.g. Bloor & Gerrard (1966) [8], McKillop & Durst (1984) [24] and Noca *et al.* (1998) [26]. Interestingly, the careful and extensive DPIV-measurements of Noca *et al.* (1998), for ($300 < Re < 4000$), do not show in their typical time-averaged topologies of the near wake the feature of two peaks in u_{RMS} along the wake centerline. Instead, their typical topology shows a behaviour for u_{RMS} along the wake centerline which is similar to the present ones for $Re \geq 8000$ (Flavio Noca, California Institute of Technology, personal communication 1998). The reasons for this disparity are unclear.

There was a significant increase in the maximum streamwise RMS velocity in between $Re = 1.5 \times 10^3$ and $Re = 5.0 \times 10^3$; at higher Re this level became virtually constant ($\hat{u}_{RMS} \simeq 0.44$). For all Re the maximum spanwise RMS velocity ($\hat{w}_{RMS}$) was practically constant. The length ℓ_S, the position for maximum skewness of the streamwise velocity fluctuations S_u, was close to the mean value between $\ell_u^{(1)}$ and $\ell_u^{(2)}$ (the second zero-crossing for S_u occurred just slightly upstream of the wake closure point).

Some notable features were found from plots with the streamwise coordinate scaled with the wake closure distance (not shown). With this scaling the distributions for $Re < 8 \times 10^3$ all showed a remarkable collapse, especially within regions $x/\ell_c \geq 1$. For instance, the mean velocities for $Re/10^3 = 1.5$, 3.0 and 5.0 at $x/\ell_c = 3$ were all equal to $U = 0.78$. The corresponding values for $Re/10^3 = 8$ and 10 were 0.76 and 0.74, respectively. As shown in Cantwell & Coles (1983) [11] the centerline mean streamwise velocity in this region is roughly equal to the mean streamwise celerity of the Kármán vortices. In particular for the skewness factor S_u, the scaling with ℓ_c produced a distinct grouping in between distributions for $Re < 8 \times 10^3$ and $Re \geq 8 \times 10^3$, respectively.

The LDV-results of McKillop & Durst [24], for $Re = 14 \times 10^3$, did not show up favourably in comparison with the present results, see Fig. 1(a). For instance, McKillop & Durst report $\ell_c = 1.65$ which is about 9% higher than the present value at $Re = 10 \times 10^3$. As shown in Fig. 2(a) there is actually a trend of decreasing ℓ_f ($\simeq \ell_c$) with increasing Re all the way from $Re \simeq 1.5 \times 10^3$ to the upper end of the subcritical regime ($Re \simeq 200 \times 10^3$). Presumably the disparity between the present results and those of McKillop & Durst are combination effects related to the notable differences in (i) free stream conditions

(McKillop & Durst have an oncoming free stream turbulence level of $Tu = 2.3\%$; present: $Tu = 0.1\%$), (ii) blockage ratios (10%; 1.5%) and (iii) aspect ratios ($L = 10.5$; $L = 65$).

The present results were also compared with the three-dimensional simulations as provided in Beaudan & Moin (1994) [4], for $Re = 3.9 \times 10^3$. These simulations are carried out using a spanwise computational length of 3.14 (π) diameters and statistics are compiled over approximately six vortex shedding periods. In the overall sense, the results without any subgrid-scale model were closest to the (interpolated) present data. For instance, the lengths ℓ_c and ℓ_U from this selected simulation are $\ell_c = 2.06$ and $\ell_U = 1.50$; linear interpolations in Table 1 give $\ell_c = 2.04$ and $\ell_U = 1.55$. However, the simulated minimum streamwise velocity along $y = 0$ is $U_{min} = -0.33$, which is significantly higher than the interpolated present value of $U_{min} = -0.45$ (the other three simulations have $U_{min} = -0.32$, -0.30 and -0.33, respectively). Beaudan & Moin do not state any supporting evidence for the existence of two peaks for the variation of u_{RMS} along the wake centerline.

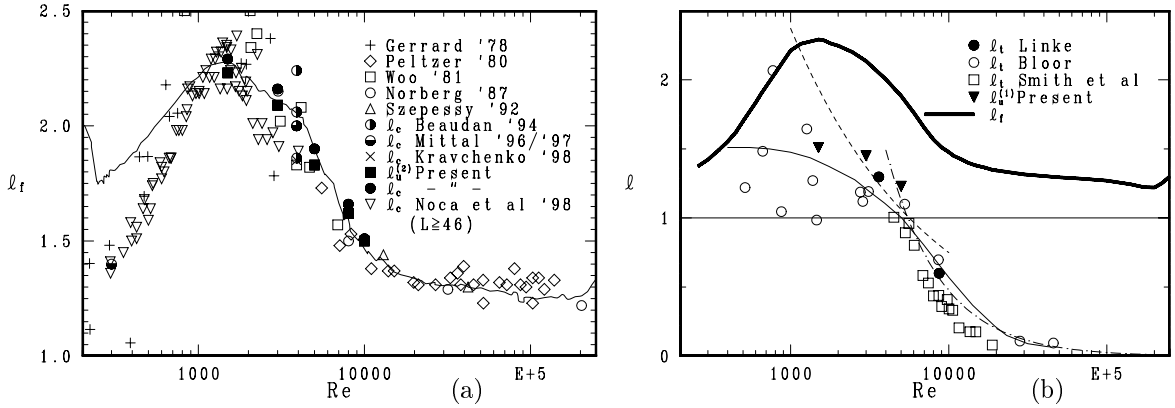

Figure 2: Streamwise length scales. (a) Vortex formation length, ℓ_f. The solid line is calculated from $\ell_f = C/(-C_{pb})$ with C described in the text. Half-filled markers are from three-dimensional numerical simulations, others are experimental. (b) Transitional length ℓ_t (indicated x-position of transition to turbulence in the shear layers), length scale $\ell_u^{(1)}$ (Table 1) and formation length ℓ_f (smoothed data from (a), solid thick line). Solid thin line: smoothed variation for ℓ_t as suggested in Bloor (1964). Broken line: $\ell_t = 75/Re^{0.5}$. Dotted line: $\ell_t = 1.1 \times (5100/Re)^{1.25}$.

As discovered by Bearman [3], the formation length roughly is inversely proportional to the base suction coefficient, i.e. $\ell_f = C/(-C_{pb})$. By using the present ℓ_f–data (ℓ_c and $\ell_u^{(2)}$) as well as results from other investigations [15, 33, 47, 28, 42, 1, 26] together with the Re-dependency for $(-C_{pb})$ from Norberg (1994) [32] it was noted that from $Re \simeq 10^3$ up to $Re \simeq 6 \times 10^3$ the C-value was approximately equal to 1.8 whereas for Reynolds numbers greater than about 7500 the value instead was about 1.6. Also the 3D-simulations in Beaudan & Moin (1994) [4], for $Re = 3.9 \times 10^3$, support the value $C = 1.8$ ($C = 1.80 \pm 0.03$). As shown by the line in Fig. 2, the formation lengths produced from the above-mentioned $(-C_{pb})$–data and by using these two levels ($C = 1.8$ and $C = 1.6$), joined smoothly with the error function centered at $Re = 6900$ ($\alpha = 4$), actually created a very reasonable variation, at least for $Re \geq 10^3$. The recent ℓ_c–data of Noca *et al.* (1998), kindly provided to the author in a personal communication with Dr. Flavio Noca (California Institute of Technology), shows that the wake closure length increases steadily from $Re = 300$ ($\ell_c \simeq 1.4$) up to a maximum of about $\ell_c = 2.3$ at $Re \simeq 1.5 \times 10^3$. Thereafter, there is a steady decrease in ℓ_c with increasing Re. On a logarithmic scale the rate of change becomes smaller at around $Re = 14 \times 10^3$ where $\ell_c \simeq 1.4$. It is worth noting, however, when using such a logarithmic scale, that the largest variations seem to occur within the interval in between $Re \simeq 5 \times 10^3$ and $Re \simeq 8 \times 10^3$. Finally, at the upper end of the subcritical regime, at $Re \simeq 200 \times 10^3$, the wake formation and wake closure occurs approximately 0.75 diameters behind the base of the cylinder ($\ell_f \simeq \ell_c \simeq 1.25$).

Fig. 2(b) shows some previously reported [21, 7, 41] experimental values for the x–position of indicated laminar/turbulent transition (at $x = \ell_t$) together with the length scale $\ell_u^{(1)}$ and a smoothed variation for the formation length ℓ_c. The thin line is the smoothed variation of ℓ_t as can be found in Bloor (1964), based on her own data and the two points as she deduced from Linke (1931). The broken line corresponds to $75/Re^{0.5}$, which is provided as a rough estimate for ℓ_t in [45], following the same line of deduction as in Roshko (1993) [38]. However, as indicated in Fig. 2(b), experimental results do not appear to follow this variation. In particular, for $Re > 5000$, approximately, the indicated point of transition seems to

move, with an increase in Re, at a much faster rate towards the separation region. The results in Smith *et al.* (1972) actually suggest a rate of change corresponding to roughly $Re^{-1.5}$. From about $Re > 5000$, the smoothed line from Bloor (1964) corresponds to a variation roughly as Re^{-1}. In both Bloor (1964) and Smith *et al.* (1972) the length ℓ_t is determined from the first appearance of transitional waves in the separated shear layers. The flow degenerates to turbulence immediately afterwards [7]. In Linke (1931) [21] the transitional point is determined from the position where the thickness of the shear layer starts to deviate from a $x^{1/2}$–variation. No value is reported for the free stream turbulence level. In Bloor (1964) the free stream turbulence level is very low, $Tu = 0.03\%$ whereas the typical value reported in Smith *et al.* (1972) is $Tu = 0.2\%$ ($Tu = 0.18 - 0.27\%$). As evident from numerous investigations, e.g. see [14, 28], the transitional process above $Re = 10^3$ (approx.) is strongly dependent on the free stream turbulence level as well as on other disturbances, for instance sound, in particular at around the shear-layer frequency [14, 34, 51]. As regards the level of free stream turbulence Tu it may be noted that with an increase in Tu from about 0.1% to 1.4% there is an approximate 20% decrease in the critical Reynolds number associated with the change-over from a high- to low-quality type of shedding (from $Re \simeq 5 \times 10^3$ to 4×10^3) [28]. As for the variation of ℓ_t in Smith *et al.* (1972) it therefore seems likely that the effective Re and the rate of decrease are higher than the expected ones at a still more quiet free stream condition. The broken line in Fig. 2(b), $\ell_t = 1.1 \times (5100/Re)^{1.25}$, is an attempt to highlight the indicated strong dependency of Re above $Re \simeq 5 \times 10^3$. Further aspects of the shear-layer transition and some indications on where the transition actually occurred in the present study are provided in the next sub-section.

3.2 Cross-stream profiles

Cross-stream profiles of the mean streamwise velocity at locations $x = 0.6$, 1.0 and 2.0, respectively, are shown in Fig. 3. Corresponding variations for the streamwise and spanwise RMS velocity are shown in Fig. 4. Critical values are summarized in Table 2.

$Re/10^3$	x	U_1	U_2	$y_{1/2}$	α	$\hat{u}_{RMS}$	y_p	$\hat{w}_{RMS}$
3.0	0.6	−0.05	1.31	0.60	12	0.36	0.60	0.14
5.0	0.6	−0.06	1.34	0.59	14	0.50	0.59	0.18
8.0	0.6	−0.11	1.35	0.56	11	0.63	0.57	0.23
3.0	1.0	−0.13	1.33	0.60	9.3	0.37	0.61	0.20
5.0	1.0	−0.24	1.34	0.57	8.8	0.52	0.58	0.26
8.0	1.0	−0.30	1.33	0.51	4.6	0.63	0.53	0.32
3.5	2.0	−0.14	1.09	0.35	1.4	0.48	0.27	0.35
5.0	2.0	+0.14	1.07	0.37	1.3	0.44	0.31	0.32
8.0	2.0	+0.33	1.05	0.40	1.3	0.39	0.3	0.29

Table 2: Summary of results from measurements across the wake.

Within the region from $x = 0.6$ to $x = 2.0$ the inverted mean streamwise velocity variation across the wake changes from a top-hat type ($x = 0.6$) to a Gaussian type ($x = 2.0$) of profile, see Fig. 3. In terms of the scaled coordinate x/ℓ_c the profiles cover the range from about 0.3 to 1.2.

Profiles for u_{RMS} and w_{RMS} across the wake are shown in Fig. 4. All profiles for u_{RMS} reached the maximum value $\hat{u}_{RMS}$ at some position off the centerline (at $\pm y_p$, see Table 2) whereas the maximum spanwise RMS velocity $\hat{w}_{RMS}$ occurred at the centerline ($y = 0$). Due to the shrinking of the formation region with an increase in Re, the positions for $\hat{u}_{RMS}$ occurred closer to $y = 0$. In between $x = 0.6$ and $x = 1.0$, for all three Reynolds numbers, a constant $\hat{u}_{RMS}$ was indicated. Conversely, still in this near-cylinder region but now for $\hat{w}_{RMS}$ there was instead an approximate 60% increase when passing from $Re = 3 \times 10^3$ to $Re = 8 \times 10^3$. For $Re = 8 \times 10^3$ and $x = 1.0$, a secondary peak for u_{RMS} occurring at $|y| \simeq 0.3$ can be noted, see Fig. 4(c). Presumably, this secondary peak occurs when the plane $x = 1.0$ ($x/\ell_c = 0.60$) cuts through an upstream part of the side-lobe containing the downstream local maximum of u_{RMS} in the xy–plane, which is expected to be located close to $x = \ell_u^{(2)}$, see [26, 4]. In consequence, ($x = \ell_u^{(2)}$, $y = 0$) is a saddle-point for u_{RMS} in the xy–plane [11].

The outer parts of the distributions for u_{RMS} at $x = 1.0$ show some notable features regarding the point of transition in the shear layers. At $Re = 3 \times 10^3$, when coming from outside the wake and going inwards, u_{RMS} is more or less constant until it suddenly, at around $|y| = 0.75$ rises within the region of strong shear, see Fig. 4(c). The same goes for $Re = 5 \times 10^3$ except that there is a small but detectable peak

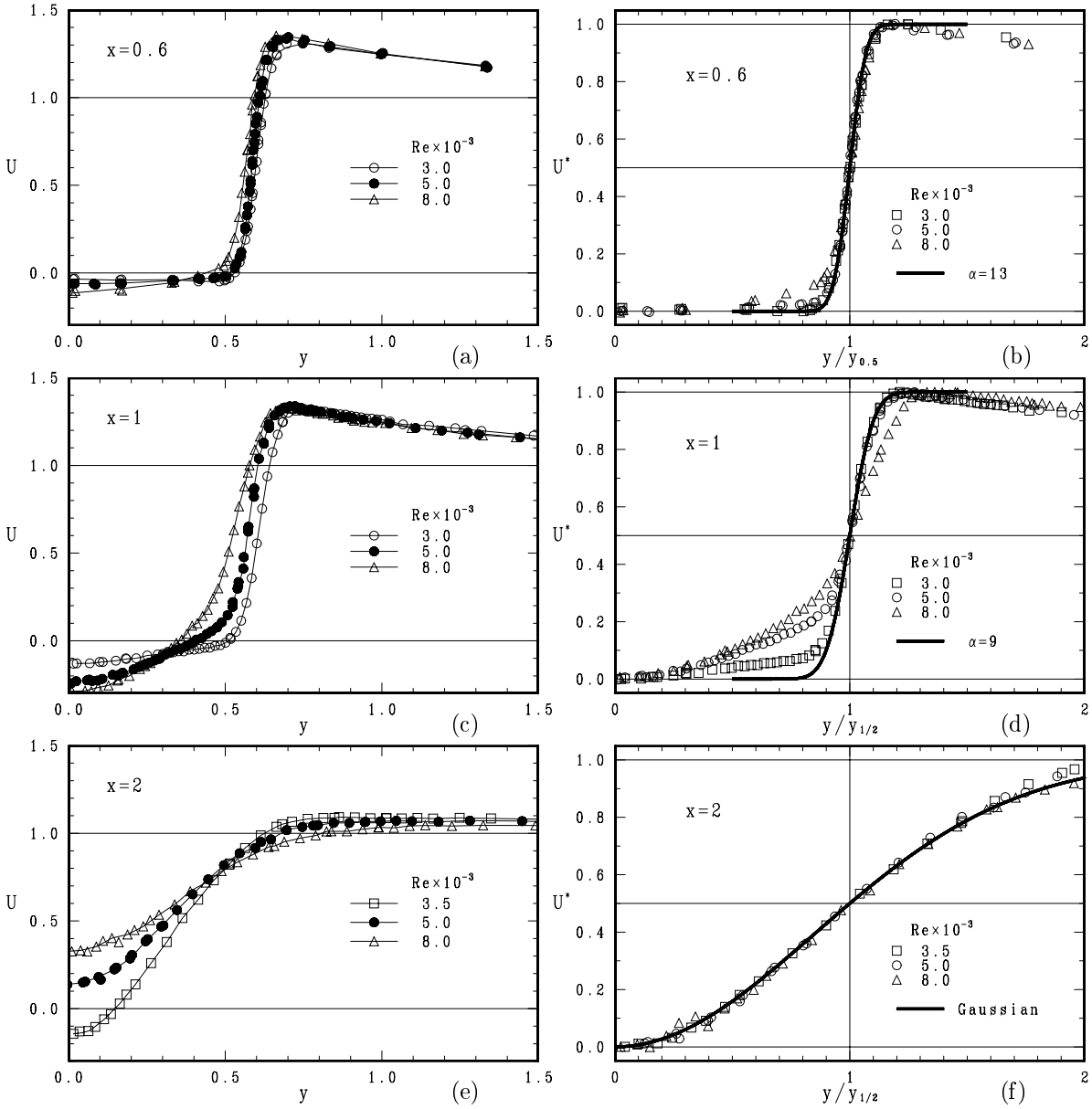

Figure 3: Mean streamwise velocity across the wake, $U vs. y$ (left) and U^* *vs.* $y/y_{1/2}$ (right) at $x = 0.6$ (a,b), $x = 1.0$ (c,d) and $x = 2.0$ (e,f). Points on the lower side of the wake ($y < 0$) have been folded.

occurring at $|y| \simeq 0.9$. The peak value is approx. $u_{RMS} = 3.7\%$. However, when the residual noise of about 1.6% from the LDV-system is taken out the level becomes 3.2%. As judged from previous studies by the author [28] the peak at around this position is due to the appearance of transition waves [7], which subsequently roll-up into shear-layer vortices and eventually degenerate into turbulence. At $Re = 8 \times 10^3$ the fluctuation level in the outer parts was considerably higher, indicating transition further upstream. Also for this case a small but detectable peak was present at $|y| \simeq 0.9$, the peak value being approx. 7.5% (7.3% without residual noise).

When the level of flow perturbation exceeds about 4% it usually marks the end of the region with exponential amplification, see Schade (1964) [39]. With this threshold value it can be inferred that the shear layer at $x = 1.0$ was laminar (non-turbulent) for $Re = 3.0 \times 10^3$, close to transition for $Re = 5.0 \times 10^3$ and finally turbulent when $Re = 8.0 \times 10^3$, in agreement with the results of Linke (1931) [21] and Bloor (1964) [7], see Fig. 2(b). From linear interpolation using corrected levels the transitional Reynolds number at $x = 1.0$ becomes $Re = 5.6 \times 10^3$. Some justification for a linear variation can be found in Prasad & Williamson (1997a) [35], where the Re–variation at $x = 1.0$ for an intermittency factor γ in the outer parts of the shear layer is reported (γ is defined as the fraction of total time when high-frequency oscillations are present). At first, up to about 85% intermittency, γ increases linearly with

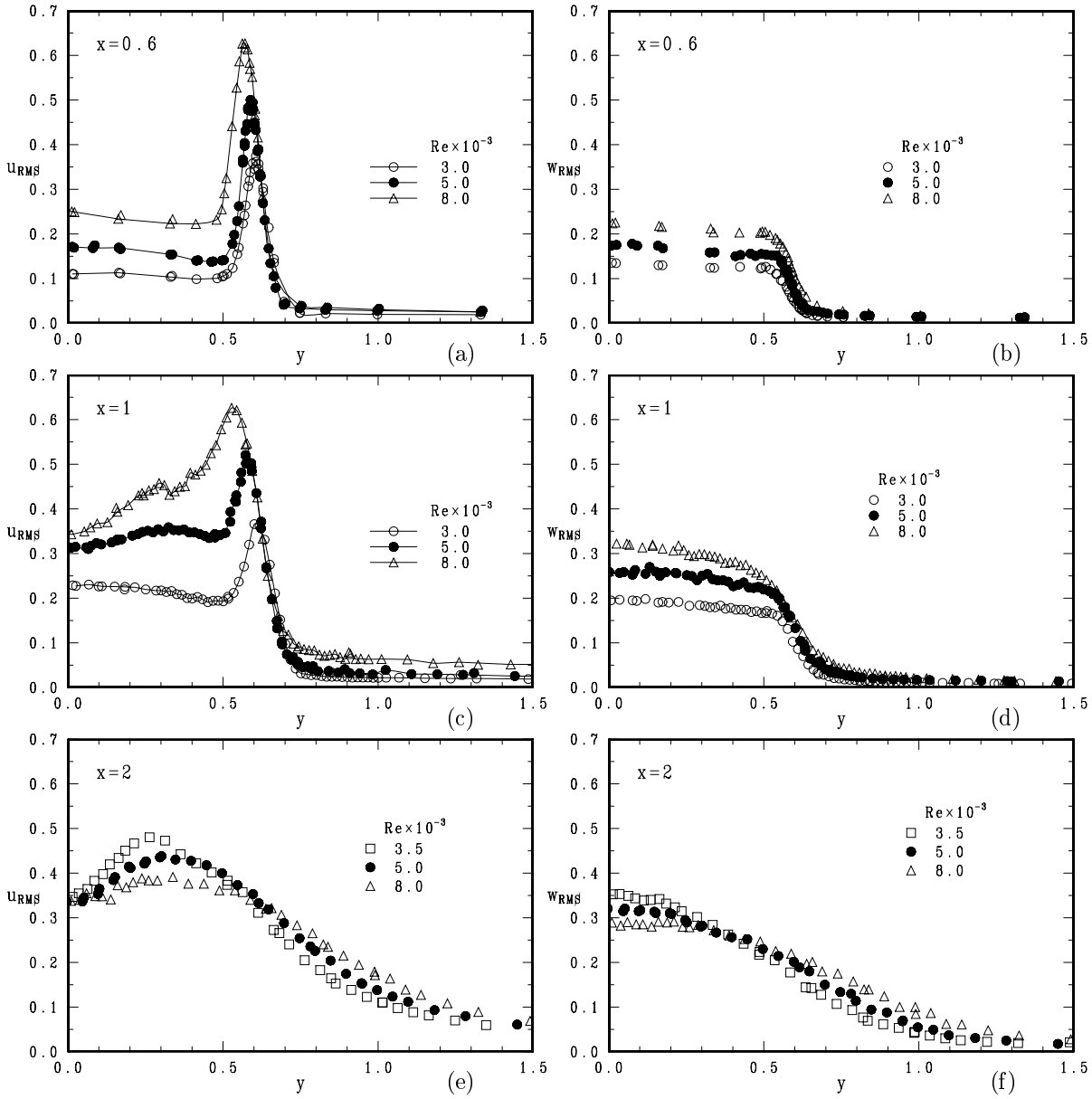

Figure 4: u_{RMS} (left) and w_{RMS} (right) across the wake at $x = 0.6$ (a,b), $x = 1.0$ (c,d) and $x = 2.0$ (e,f). Points on the lower side of the wake ($y < 0$) have been folded.

Re. In the final stages the increase towards unity is slower. From the graph at $x = 1.0$ in [35], $\gamma = 90\%$ occurs at $Re \simeq 5.6 \times 10^3$. The reported level of free stream turbulence in Prasad & Williamson (1997a) [35] is 0.08%, in parity with the present level. The agreement with the above critical Re suggests that $\gamma = 90\%$ may be used as an alternative criterion for finding the mean transitional point. The proposed approximate relation $\ell_t = 1.1 \times (5100/Re)^{1.25}$, see Fig. 2(b), is in accordance with the above analysis.

Some further aspects on shear-layer transition are provided in Chyu & Rockwell (1996) [13]. From their instantaneous near-wake vorticity fields in the xy–plane at midspan ($L = 10.3$), as taken with high-image-density PIV in water ($Tu = 0.1\%$), it can be noted that the position for appearance of distinct shear-layer vortices moves rapidly upstream with increasing Re in between $Re = 5 \times 10^3$ and $Re = 10^4$. At $Re = 5 \times 10^3$ no distinct vortices can be traced within a region $x \leq 1$. However, at $Re = 10^4$, the formation of such distinct vortices (which presumably very shortly downstream degenerate into "turbulence") seems to occur at around $x = 0.5$, in reasonable agreement with the suggested formula.

The shear parameter α in Table 2 was determined from the following procedure. For each x-station, the minimum and maximum streamwise velocities, U_1 and U_2, were used as reference values in a scaled velocity function: $U^* = (U - U_1)/(U_2 - U_1)$. The half-wake distance $y_{1/2}$ was determined from the

y-position where $U^* = 1/2$. The profiles for U^* were compared with the following function:

$$U^* = \frac{1}{2}\left[1 + \mathrm{erf}(\eta)\right], \tag{1}$$

where $\eta = \alpha\,(y/y_{1/2} - 1)$, see Fig. 3(b). From eq. 1 the maximum velocity gradient

$$\left(\frac{dU}{dy}\right)_{max} = \frac{U_2 - U_1}{\sqrt{\pi}}\,\frac{\alpha}{y_{1/2}} \tag{2}$$

occurs at $y = y_{1/2}$. The profiles were compared in two ways with the above shear-layer velocity function. The first involved a least-square fit to eq. 1 over parts of the profile. In the other the value for α was calculated from the maximum velocity gradient using eq. 2. In the first method the velocities outside the point where the velocity starts to decrease were taken out. The least-square fit was then applied in between $U^* = 0.4$ and $U^* = 1.0$. To within $\pm 6\%$ the two methods gave out the same shear parameter. Table 2 contains the mean value between the two methods, notwithstanding an indicated higher accuracy for the first method.

There was a significant drop in the shear parameter occurring in between $x = 0.6$ and $x = 1.0$, especially for $Re = 8 \times 10^3$. As described earlier, for $Re = 8 \times 10^3$, the transition to turbulence in the shear layer is indicated to occur in between these x–stations. The drop in α at $x = 0.6$ in between $Re = 5 \times 10^3$ and $Re = 8 \times 10^3$ suggests that the mean point of transition at $Re = 8 \times 10^3$ occurs slightly downstream of $x = 0.6$.

The profiles were also tested against the functional shear velocity profile as used in Monkewitz & Nguyen (1987) [25]. This type of profile contains a "shape parameter" N. It is suggested from stability considerations that the absolute instability for wake profiles is initiated when $N = 12.5$ [25]. When tested against the present data the optimum N-values were found to be more or less equal (within $\pm 6\%$) to the shear parameter α. The uncertainty for the reported values of α in Table 2 was estimated to be $\pm 10\%$. It is inferred in Monkewitz & Nguyen (1987) that the basic instability frequency, the von Kármán frequency, is inversely related to the half-width $y_{1/2}$ at the position for change-over between a convectively and absolutely unstable region in the separating shear layers. In a non-dimensional form the predicted transition point frequency is equal to $1.68/(4\pi\, y_{1/2})$ [25]. When applied to $x = 0.6$ at $Re = 3 \times 10^3$, for which $N \simeq \alpha = 12$ and $y_{1/2} = 0.60$, the frequency is 0.22. This is about 6% higher than the reported experimental Strouhal number at this Re ($St = 0.210 \pm 0.002$ [32]). Considering the uncertainties involved this may look as an reasonable deviation. However, when applied to $x = 0.6$ for $Re = 8 \times 10^3$ ($N \simeq 11$) the frequency becomes 0.24, which is more than 15% higher than the experimental value. The relatively high uncertainty in α does not seem to alter this increasing discrepancy with increasing Re. To match the experimental Strouhal number for $Re = 8 \times 10^3$ ($St \simeq 0.203$), the value $y_{1/2} \simeq 0.66$ is needed, which for $x < 0.6$ seems highly unlikely to occur. Apparently, the drop in St over this range of Re cannot be predicted with this procedure.

4 Final Discussion

The present study shows that there is a marked difference in between results for $Re < 8 \times 10^3$ and $Re \geq 8 \times 10^3$, respectively. This seems to be directly related to the transition from high- to low-quality vortex shedding which for sufficiently large aspect ratios and in a smooth oncoming free stream is initiated at around $Re = 5 \times 10^3$ [31]. It is suggested herein that the actual transition might be due to a resonance between spanwise length scales of secondary near-wake instabilities. As shown e.g. in Refs. [28, 29] there is a peak in the near-cylinder spanwise correlation of velocity fluctuations occurring at around the transitional Reynolds number, suggesting some kind of a near-wake resonance. It is also suggested that the proposed resonance has a direct influence on the transition from laminar to turbulent flow in the separating shear layers.

The mode B vortices are initiated at around $Re = 230$ [45] and they have been shown to exist up to at least $Re = 21 \times 10^3$ [2]. The mean spanwise distance between these longitudinal structures, the wavelength λ_z^B, is of the order one cylinder diameter, irrespective of the Reynolds number. Having survived the transition at around $Re = 5 \times 10^3$ it seems very likely that these rib-like structures are present in the whole subcritical regime, perhaps for all $Re > 230$. A collection of previous results for λ_z^B [44, 54, 10, 49, 20, 12] is shown in Fig. 5(b) (unfilled markers). The results in [49] suggest that there is a slight decrease in λ_z^B with increasing Re. However, based on the observations in [2] and [12],

λ_z^B is likely to remain at around unity or slightly below, up to at least $Re = 21 \times 10^3$. As shown by e.g. Brede *et al.* (1996) [10] the rib-like mode B vortices develop very close to the base of the cylinder. Further, as evidenced in Lin *et al.* (1996) [20] for $Re = 5 \times 10^3$ and $Re = 10^4$ at $x = 1$, the mode B structures manifest themselves in particular at instants separated by one-half Kármán cycle, when irrotational fluid is drawn across the wake. As suggested by Williamson [45] the mode B structures is caused by an mixing layer type of instability that scales on the thickness of the braid region. Due to axial stretching the streamwise vorticity amplifies strongly in these connecting braid regions.

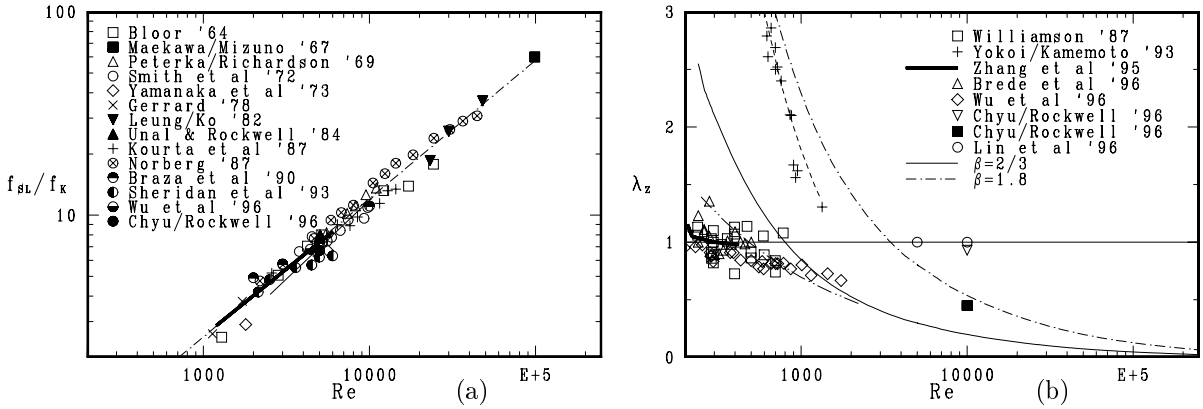

Figure 5: (a) Ratio between the shear layer frequency and the von Kármán frequency, f_{SL}/f_K. Solid thin line: $A = 0.0096$, $n = 0.773$ (Wei & Smith '86, lumped anemometry data). Thick solid line: $A = 0.0269$, $n = 0.6587$ (Prasad & Williamson '96). Dotted line: $A = 0.023$, $n = 0.68$ (present correlation). (b) Spanwise length scales. Broken line: $1800/Re$; double-dotted line: $22/Re^{0.5}$ as suggested from Mansy *et al.* '94 ($x = 3$); λ_z^{SL} from eqns. (3,4) with $\beta = 1.8$ (dotted line) and $\beta = 2/3$ (thin line). The unfilled marker of Chyu & Rockwell '96 represents their value at $x = 1.5$ whereas the filled marker is for $x = 0.5$.

Another important feature in the near wake is the development of shear-layer vortices in the separating shear layers, which show up at around $Re = 1200-1800$ [35]. As shown in Fig. 5(a) the ratio between the observable shear-layer frequency f_{SL} and the von Kármán frequency f_K varies approximately according to: $f_{SL}/f_K \simeq A \times Re^n$. A least-square fit to the data in Fig. 5(a) [7, 22, 34, 41, 51, 15, 19, 18, 28, 9, 40, 50, 13] gave ($A = 0.023$, $n = 0.68$), in agreement with Prasad & Williamson (1997a) [35].

The streamwise wavelength of this instability, λ_x^{SL}, is equal to its local streamwise convection velocity divided by f_{SL}. Since the instability is initiated in the separating shear-layers the convection velocity can be approximated as half the value of mean velocity at separation, which in turn for sufficiently high Re can be estimated as $\sqrt{1 - C_{pb}}$ [37, 46]. As a further justification, the ratio between U_2 at $x = 0.6$ from Table 2 and $\sqrt{1 - C_{pb}}$ from [32] is 0.96 ± 0.01. The approximate formula for the mean streamwise wavelength becomes:

$$\lambda_x^{SL} \approx \frac{\sqrt{1 - C_{pb}}}{2 \times St \times A \times Re^n} \tag{3}$$

where $St = f_K$ is the Strouhal number. When using the data for St and $-C_{pb}$ from [32] and values for A and n as above the wavelengths for Reynolds numbers in Table 1 are: 0.95, 0.61, 0.45, 0.34, 0.30 ($Re/10^3 = 1.5$, 3, 5, 8, 10). The last three wavelengths ($Re/10^3 = 5$, 8, 10) can be compared with results from a PIV-study by Chyu & Rockwell (1996) [13]. From visual inspection of instantaneous spanwise vorticity contours in [13] the wavelengths are approximately: $\lambda_x^{SL} = 0.43$, 0.28 and 0.23, respectively. When considering the approximations and uncertainties involved the wavelengths from eq. 3 seem to be in fair agreement with the measurements. The question now is to find a relation between λ_x^{SL} and its spanwise counterpart, λ_z^{SL}. In symbolic form a factor β can be introduced:

$$\lambda_z^{SL} = \beta \times \lambda_x^{SL} \tag{4}$$

For observable shear-layer vortices, what is the most relevant value for β? In many contexts, e.g. see [46], the value of $\beta = 2/3$ is introduced. The solid thin line in Fig. 5(b) corresponds to this value and as seen, also see [46, 50], there is a match with λ_z^B occurring at around $Re = 10^3$. Actually, there is

a correspondence between λ_z^{SL} using $\beta = 2/3$ and a thought extension to higher Re for the spanwise correlation lengths as measured at $x = 3$ by Mansy *et al.* (1994) [23], see Fig. 5(b). Nevertheless, the value of $\beta = 2/3$ appears to be relevant for free shear layers at the inception of pairing or merging between vortices [17]. However, no merging is detectable for the shear-layer vortices in the separated shear layers close to the cylinder [12]. From PIV measurements at $Re = 10^4$ as presented in [12] a value of $\beta = 1.9$ is reported, which is in general agreement with the ratio found during the initial stage of development of a mixing layer, which ranges from about $\beta = 1.6$ [17] to $\beta = 2.0$ [5]. The dotted line in Fig. 5(b) corresponds to $\beta = 1.8$, which seems to be a reasonable estimate. For $Re = 5 \times 10^3$ when using $\beta = 1.8$ the indicated spanwise wavelength of shear-layer vortices is $\lambda_z^{SL} \approx 0.8$, which is about the same value as indicated from measurements of the spanwise wavelength of mode B-vortices, see Fig. 5(b). Interestingly, the spanwise distance between "spread spots", as noted in Yokoi & Kamemoto (1992/3) [52, 53] for $200 < Re \leq 1340$ ($L = 20, 40$), roughly follows the indicated variation of λ_z^{SL}, see Fig. 5(b). These large-scale spanwise deformations, which as yet have not been confirmed by others, might then be due to interactions between unstable mode A instabilities [16] and shear-layer transitional waves [7].

It is tempting from the above to suggest that the transition at around $Re = 5 \times 10^3$ is due to a resonance condition met between λ_z^{SL} and λ_z^B, i.e. $\lambda_z^B = \lambda_z^{SL} \approx 0.8$. Interestingly but maybe fortuitous the mode B instability at onset has $\lambda_z^B = 0.82$, see Henderson (1997) [16]. An equality in scales does not imply that a resonance actually will occur, the vortical structures also have to be in close proximity to each other. This seems to be the case. As noted earlier the inception of mode B structures occurs very close to the cylinder. At these Re, due to the shrinking of the formation region, the connecting braid between primary structures will be in close proximity to the separating shear layers, with a significant amount of wake swinging. From Fig. 2(b) the laminar/turbulent transition in the shear layers occurs at $x \simeq 1.1$ while the first peak in the distribution of u_{RMS} along $y = 0$, which is probably due to the crossing of B mode longitudinal structures (Section 3.1), occurs at $x = 1.23$ (Table 1). At this point and at lower Re as well, the first peak in u_{RMS} along $y = 0$ appears to be connected to the point of laminar/turbulent transition, see Fig. 2(b). As the longitudinal structure is swinging together with the Kármán vortex at its upstream side [2] there is a possibility for a direct interaction between the secondary structures, with a possible subsequent break-up into turbulence. As the suggested interaction occurs close to the cylinder it also involves the primary instability, which then might affect the whole shedding process. As from about this particular $Re \simeq 5 \times 10^3$ the mean point of laminar/turbulent transition moves upstream with an increasing rate with an increase in Reynolds number (Fig. 2(b)), which appears to be directly related to the proposed near-wake transitional behaviour.

Conclusions

The measurements provide further evidence for the existence of a fundamental transition at around $Re = 5 \times 10^3$. Some possible reasons for this transition to show up and its consequences regarding the near wake flow are discussed. There exists two peaks in the distribution of RMS streamwise velocity along the wake centerline for $1.5 \leq Re/10^3 \leq 5$ whereas only one such peak is present at higher Reynolds numbers ($8 \leq Re/10^3 \leq 10$). At these higher Re the first peak, which is upstream of the highest one, degenerates into an inflexional point. The first peak and the inflexional point is probably connected to the cross-over of mode B longitudinal vortices. A possible equality of spanwise scales for mode B vortices and shear-layer vortices at around $Re \simeq 5 \times 10^3$ is noted.

Acknowledgements

The author wish to thank Dr. Gunnar Johansson and Lic. Eng. Hans Rydholm for introducing me to the LDV-system and for their helpful advice.

References

[1] Balachandar, S., Mittal, R., and Najjar, F. M. *J. Fluid Mech. 351* (1997), 167–199.

[2] Bays-Muchmore, B., and Ahmed, A. *Phys. Fluids A 5*, 2 (1993), 387–392.

[3] Bearman, P. W. *J. Fluid Mech. 21*, 2 (1965), 241–255.

[4] Beaudan, P., and Moin, P. Report TF-62, Stanford University, Stanford, CA 94305, Dec. 1994.

[5] Bell, J. H., and Mehta, R. D. *J. Fluid Mech. 239* (1992), 213–248.

[6] Blevins, R. D. *J. Fluid Mech. 161* (1985), 217–237.

[7] Bloor, M. S. *J. Fluid Mech. 19*, 2 (1964), 290–304.

[8] Bloor, M. S., and Gerrard, J. H. *Proc. Roy. Soc. (London), Ser. A 294* (1966), 319–342.

[9] Braza, M., Chassaing, P., and Ha Minh, H. *Phys. Fluids A 2*, 8 (1990), 1461–1471.

[10] Brede, M., Eckelmann, H., and Rockwell, D. *Phys. Fluids 8*, 8 (1996), 2117–2124.

[11] Cantwell, B., and Coles, D. *J. Fluid Mech. 136* (1983), 321–374.

[12] Chyu, C. K., and Rockwell, D. *J. Fluid Mech. 320* (1996), 117–137.

[13] Chyu, C. K., and Rockwell, D. *J. Fluid Mech. 322* (1996), 21–49.

[14] Gerrard, J. H. *J. Fluid Mech. 22*, 1 (1965), 187–196.

[15] Gerrard, J. H. *Phil. Trans. Roy. Soc. London, Ser. A 288*, 1354 (Mar. 1978), 351–382.

[16] Henderson, R. D. *J. Fluid Mech. 352* (1997), 65–112.

[17] Huang, L. S., and Ho, C. M. *J. Fluid Mech. 210* (1990), 475–500.

[18] Kourta, A., Boisson, H. C., Braza, M., and Ha Minh, H. In *Turbulent Shear Flows 5, Proc. Cornell Univ. 1985* (1987), pp. 83–97.

[19] Leung, C. T., and Ko, N. W. M. In *Heat Transfer 1982, München* (1982), Hemisphere, pp. 229–232.

[20] Lin, J. C., Vorobieff, P., and Rockwell, D. *Phys. Fluids 8*, 2 (1996), 555–564.

[21] Linke, W. *Physik. Zeitschr. 32* (1931), 900–914.

[22] Maekawa, T., and Mizuno, S. *Phys. Fluids Suppl.* (1967), 184–186.

[23] Mansy, H., Yang, P. M., and Williams, D. R. *J. Fluid Mech. 270* (1994), 277–296.

[24] McKillop, A. A., and Durst, F. In *Laser Anemometry in Fluid Mechanics II* (1984), Ladoan Lisboa, Portugal, pp. 329–346.

[25] Monkewitz, P. A., and Nguyen, L. N. *J. Fluids & Struct. 1*, 2 (1987), 165–184.

[26] Noca, F., Park, H., and Gharib, M. In *Advances in the Understanding of Bluff Body Wakes and Vortex-Induced Vibration, Washington D.C.* (June 1998), ASME.

[27] Norberg, C. *J. Wind Eng. Ind. Aero. 23* (1986), 501–514.

[28] Norberg, C. Publ. 87/2, Appl. Thermodyn. & Fluid Mech., Chalmers Univ., Sweden, May 1987.

[29] Norberg, C. In *Proc. Fourth Asian Congress of Fluid Mechanics, Hong Kong* (Aug. 1989), Suppl. Vol.

[30] Norberg, C. In *Proc. 11th Australasian Fluid Mechanics Conference, Hobart* (Dec. 1992), vol. 1, pp. 507–510.

[31] Norberg, C. In *Bluff-Body Wakes, Dynamics and Instabilities, Proc. IUTAM Symp. Göttingen, Sept. 1992* (1993), Springer-Verlag, pp. 275–278.

[32] Norberg, C. *J. Fluid Mech. 258* (1994), 287–316.

[33] Peltzer, R. D., and Rooney, D. M. *ASME J. Fluids Eng. 107* (1985), 86–91.

[34] Peterka, J. A., and Richardson, P. D. *J. Fluid Mech. 37*, 2 (1969), 265–287.

[35] Prasad, A., and Williamson, C. H. K. *J. Fluid Mech. 333* (1997), 375–402.

[36] Prasad, A., and Williamson, C. H. K. *J. Fluid Mech. 343* (1997), 235–265.

[37] Roshko, A. NACA TN 3168, National Advisory Committee for Aeronautics, Washington D.C., 1953.

[38] Roshko, A. *J. Wind Eng. Ind. Aero. 49* (1993), 79–100.

[39] Schade, H. *Phys. Fluids 7* (1964), 623–628.

[40] Sheridan, J., Soria, J., Wu, J., and Welsh, M. C. In *Bluff-Body Wakes, Dynamics and Instabilities, Proc. IUTAM Symp. Göttingen, Sept. 1992* (1993), Springer-Verlag, pp. 115–118.

[41] Smith, R. A., Woo Taik Moon, and Kao, T. W. *ASME J. Basic Eng. 94* (1972), 771–776.

[42] Szepessy, S., and Bearman, P. W. *J. Fluid Mech. 234* (1992), 191–217.

[43] Unal, M. F., and Rockwell, D. *J. Fluid Mech. 190* (1988), 491–512.

[44] Williamson, C. H. K. *Bull. Am. Phys. Soc. 32* (1987), 2098.

[45] Williamson, C. H. K. *Ann. Rev. Fluid Mech. 28* (1996), 477–539.

[46] Williamson, C. H. K., Wu, J., and Sheridan, J. *Phys. Fluids 7*, 10 (1995), 2307–2309.

[47] Woo, H. G. C., Cermak, J. E., and Peterka, J. A. Tech. Rep. CER81-82HGCW-JEC-JAP7, Colorado State University, July 1981.

[48] Wu, J., Sheridan, J., and Welsh, M. C. *ASME J. Fluids Eng. 118* (1996), 531–536.

[49] Wu, J., Sheridan, J., Welsh, M. C., and Hourigan, K. *J. Fluid Mech. 312* (1996), 201–222.

[50] Wu, J., Sheridan, J. Hourigan, K., and Soria, J. *Exp. Thermal & Fluid Science 12*, 2 (1996), 169–174.

[51] Yamanaka, G., Imaichi, K., and Adachi, T. *DISA Information No. 14* (1973), 37–44.

[52] Yokoi, Y., and Kamemoto, K. *JSME Int. Journal, Ser. II 35*, 2 (1992), 189–195.

[53] Yokoi, Y., and Kamemoto, K. *JSME Int. Journal, Series B 36*, 2 (1993), 201–206.

[54] Zhang, H. Q., Fey, U., Noack, B. R., König, M., and Eckelmann, H. *Phys. Fluids 7*, 4 (1995), 779–793.